UNDERWATER FRAGMENTATION OF CYLINDERS

J. J. Lee[1] and G. Rude[1]

[1] *Defence R&D Canada – Suffield*
PO Box 4000, Station Main, Medicine Hat, Alberta, T1A 8K6, Canada

ABSTRACT

Because underwater explosion fragments have a limited range of propagation, fragment damage from cased underwater charges has not been considered a serious threat. With recent interest in asymmetric threats and close-proximity improvised explosives, there is renewed interest in the fragmentation properties of cased underwater explosives, particularly in shallow depths where fragments can be launched out of the spray dome into the air. The present paper examines the fragmentation characteristics of metal cylinders filled with explosive and detonated underwater. The fragmentation process was filmed using high-speed video, revealing a fragment cloud closely confined to the detonation product bubble. However, small protrusions appearing on the bubble surface at later times may indicate fragments pulling ahead of the bubble interface. Fragment samples were recovered after the test, and the size distributions showed a non-Gaussian trend with the fragment masses significantly larger than in air. As expected, the fragment velocities decayed quickly due to water drag, limiting the damage threat to very short distances from the charge. This study provides some insight into the underwater fragmentation process and damage potential of the fragments.

INTRODUCTION

The present work consists of a preliminary investigation of the characteristics of underwater fragmentation. Trials were performed on steel cylinders filled with a high explosive and detonated underwater. Fragmentation properties such as fragment size and velocity were measured using fragment collection and high-speed underwater video images of the explosion.

Underwater explosive fragmentation has received little attention compared to fragmentation in air due in part to the perception that fragments or projectiles do not propagate in a dense liquid medium such as water. While water can provide an effective barrier for stopping fragments such as in ordnance disposal operations [1], a sufficiently large cased explosive detonated at a sufficiently shallow depth can disperse fragments and generate a blast wave both above and below the surface [2,3]. A relatively new concern is the potential damage caused by an underwater cased charge in very close proximity to a ship or other naval platform. This situation may arise as a result of an asymmetric attack [4] where an Improvised Explosive Device (IED) can be transported very near an in-port vessel by a small boat or diver and be detonated. If the charge is cased or contains fragmenting materials, damage can be caused by many mechanisms including underwater blast and fragment impact.

To investigate the possible threat of underwater fragments, the basic fragmentation properties of a simplified cased charge are examined in the present work. A simple experimental

arrangement was conceived to test small steel cylinders filled with explosive. The fragmentation process was filmed underwater using a high-speed camera, and fragments were collected after each test for analysis. The preliminary results on fragment size and velocity provided some insight into the possible threat posed by the fragments.

EXPERIMENTAL DETAILS

Four tests were conducted with identical charges: three underwater and one in the air for comparison. The charge consisted of a mild steel cylinder with an outer diameter of 67 mm, and inner diameter of 35 mm, and a length of 92 mm (Figure 1). The cylinder was filled with 143 g ± 1 g of C4 explosive (91% RDX by mass), and a Reynolds RP-83 detonator was inserted in the center of the explosive core. The tip of the detonator was approximately at the center of the charge.

Figure 1. Explosive charge filled with C4 and fitted with a blasting cap (white wires shown).

The first underwater test was conducted in a commercially-available plastic garbage can with a volume of 189 liters. The can was approximately 1.2 m high with a 35 cm by 35 cm cross section. The charge was placed on a stand in a vertical orientation at a depth to the charge center of about 35 cm below the surface. The 2nd and 3rd tests were conducted in small swimming pools about 4.6 m in diameter and filled with water to a depth of about 1.2 m. For the 2nd test , the charge was placed on a stand in a horizontal orientation at a depth of about 45 cm. For the 3rd test, the charge was placed in a vertical orientation, also at a depth of 45 cm. During each underwater test, the garbage can or pool was destroyed by the explosion. The final test was conducted in air on a small wooden table.

The two main underwater tests (2nd and 3rd) and the test in air were filmed using a high-speed digital video camera at a rate of 10,000 frames/sec (100 μs/frame). A special waterproof and blast-resistant camera housing was used in the underwater tests. Tourmaline crystal gauges (model# TR-2 from Neptune Sonar) were used to measure the underwater free-field pressure.

Because the fragments were not expected to propagate far beyond the immediate vicinity of the charge, collections were taken on the ground at the location of the explosion after each test. For the test in air, fragments were collected using a 3-m high stack of square Donnacona™ (a light, wood fiber-based material) panels 1.2 m in dimension.

RESULTS AND DISCUSSION

Fragment Velocity

The underwater explosion process was found to produce a cloud of fragments that interacted closely with the detonation product bubble. In the early stages, the detonation of high explosive proceeded quickly to completion within 5-10 μs due to the rapid detonation velocity in C4 of about 8 mm/μs. The subsequent explosion process was observed in high-speed video images (Figure 2). The end view shows the cylindrical charge appearing as a small circle resting on the vertical support stand (0 ms frame). After detonation, the product bubble begins to grow, appearing as a dark circle in the images. At 0.2 ms, small white protrusions appear on the surface of the bubble suggesting that fragments have pulled ahead of the interface between the detonation products and the water. At 0.3 ms, the protrusions collapse into short, dark tracks giving the bubble a hairy appearance. At later times, the fragment tracks do not lengthen, but follow the natural growth of the bubble, suggesting that the fragments do not outdistance the bubble boundary, but instead follow the flow as the water is being pushed outwards by the bubble expansion. Subsequent bubble growth and collapse may influence fragment motion. However the period was calculated to be about 160 ms from scaling laws [5], and since surface cavitation was found to obscure the view of the explosion phenomena beyond 1 ms after detonation, these effects could not be observed.

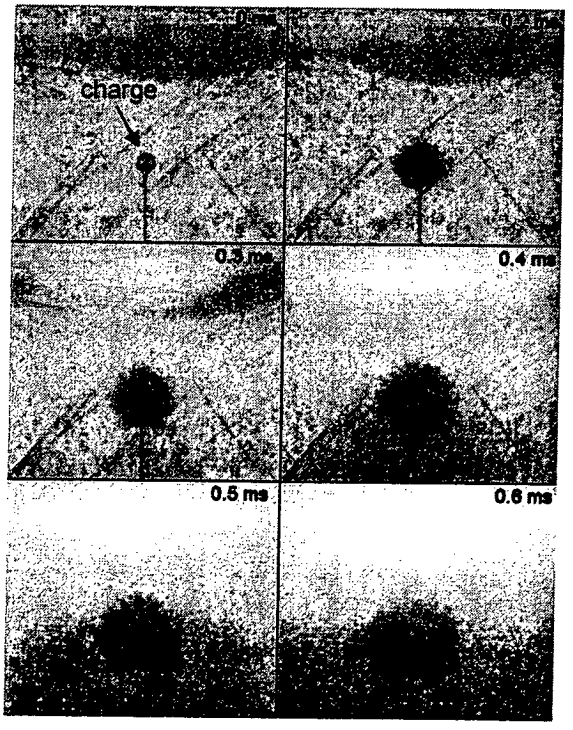

Figure 2. Series of frames from high-speed video imaging of exploding underwater charge.

By measuring the radius of the bubble from the video images, a growth rate was estimated and found to be 196 m/s (Figure 3). Calculating the initial fragment velocity (V_m) using the Gurney method shown in Eq. 1 [6]:

$$V_m = \sqrt{2E}\left(\frac{M}{C}+\frac{1}{2}\right)^{-1/2} \quad (1)$$

where $\sqrt{2E}$ is the Gurney constant of 2.68 mm/μs for C4, M is the casing mass, C is the explosive mass, we obtain a value of 730 m/s. Although this value is valid for explosions in air, it is used here as a preliminary estimate of the initial breakout velocity of the fragments. That the Gurney velocity is over three times higher than the bubble growth rate further supports the fact that fragments rapidly decelerate after pulling ahead of the bubble interface and subsequently follow the water flow surrounding the bubble.

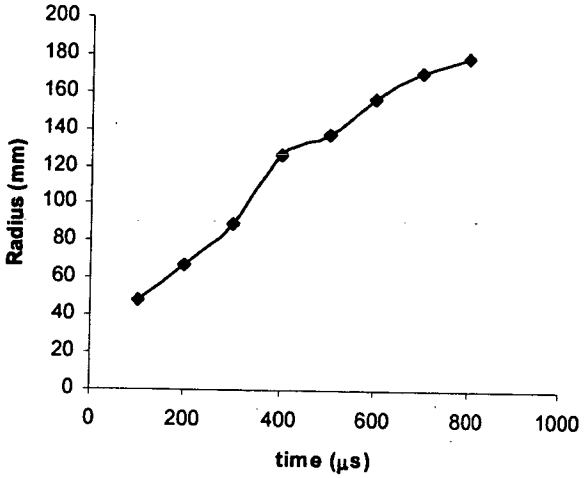

Figure 3. Growth of the underwater explosion bubble.

An image from video footage of the 3rd underwater test shows a side view of the explosion process (Figure 4). In this test, the cylinder was placed vertically, and the view of the charge was from the side rather than the end. The explosion bubble was found to be hourglass-shaped. This is believed to be due to the expulsion of detonation products out the open ends of the cylinder during the early stages of the explosion, setting up a vertically-directional flow field. After the fragments have crossed the bubble interface, the bubble proceeds to grow in a more spherical manner as the waist of the hourglass expands and the ends assume a rounder shape.

Figure 4. Side view of the underwater explosion.

A high-speed video camera located outside the pool captured the growth of the spray dome and fragments expelled from the water (Figure 5). As the spray dome grew, fragments were expelled from the surface, forming small trails of spray where they broke out of the dome. The exit velocity was likely affected by complex mechanisms as the fragments traveled through cavitated water and the spray dome, which consisted of a highly heterogeneous mixture of air and water droplets.

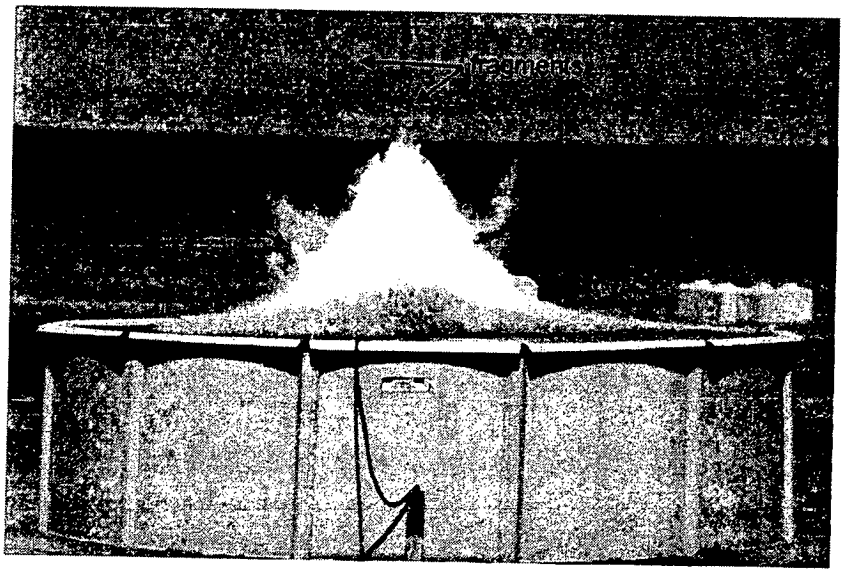

Figure 5. View of the pool during the 2nd underwater explosion test.

Fragment Size

The fragments collected after the tests were found to have typical casing fragment shapes such as elongated strips or rectangular sharp-edged blocs (Figure 6). It was found that although most of the fragments did remain in a localized area around the explosion origin, certain larger fragments were found at distances of over 100 m away. These larger fragments were likely expelled from the water into the air. During collection, the smaller fragments were not found, and may have been washed away by water rushing out of the explosion-damaged pool.

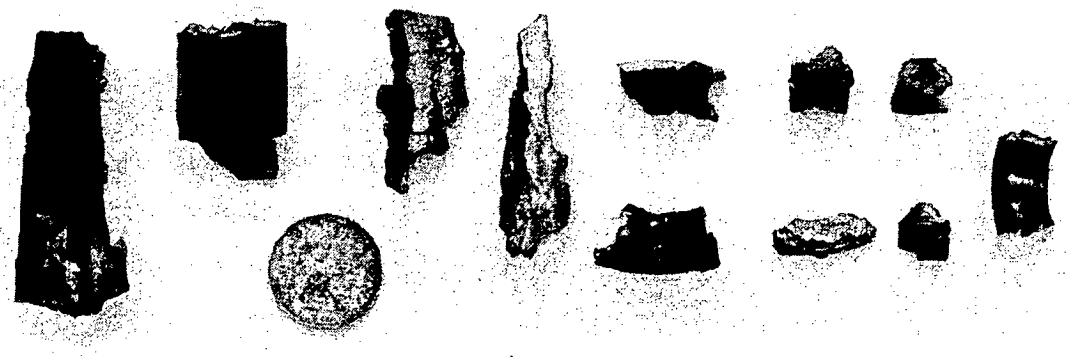

Figure 6. Underwater explosion fragments with a Canadian one dollar coin shown for scale.

The fragments from each test were individually weighed for analysis, and the results are shown in Table 1 below. The three underwater tests are labeled "U/W" and the test in air was labeled "Air". Due to the smaller amount of water in the first test, fewer fragments were found as they were dispersed to further distances. The results show that the average underwater fragment size ranged from 15 g to 36 g, and the average size in air was 7.5 g. The wide variation of the average sizes is likely due to inconsistencies in the fragment collection method. For example, a larger portion of smaller fragments may have been found during the second test, lowering the value of the average. Since discrepancies in the recovered fragments occurred mostly for smaller fragments, the largest fragment (M_{big}) better represents the general fragment size. The largest fragment sizes were found to vary less from test-to-test, and were found to be 3-4 times larger than the largest fragment from the air explosion.

Table 1. Summary of fragment analysis.

	U/W Test#1	U/W Test#2	U/W Test#3	Air Test#4
% Mass Recovered	11%	51%	73%	13%
M_{ave} (g)	19.2	15.0	36.0	7.5
Standard Deviation (g)	19.6	19.1	27.0	6.1
M_{big} (g)	66.1	77.8	110.9	24.4
R_{Gurney}	56 cm	60 cm	71 cm	298 m
R_{Exp}	39 cm	43 cm	51 cm	198 m

The last two rows of Table 1 show the maximum range of the fragments calculated by considering the drag force. This calculation consisted of finding the distance traveled by a fragment as it is decelerated by fluid drag until it reaches a kinetic energy of 79 J, as defined by DoD 6055.9-STD as the smallest impact energy of a hazardous fragment, i.e. fragments below this critical energy are not considered dangerous. The maximum range R can be calculated using the expression [7]:

$$E_{cr} = 0.5mv_0^2 e^{-\left(\frac{2R}{L_1 m^{1/3}}\right)} \tag{2}$$

where E_{cr} is the critical energy, m is the fragment mass, v_0 is the initial fragment velocity, L_1 is:

$$L_1 = \frac{2k^{2/3}}{C_D \rho} \tag{3}$$

where k is the shape factor times the fragment density, C_D is the drag coefficient, and ρ is the density of the fluid medium. Although Eqs. 2 and 3 were originally used for fragments in air, they are derived from the basic drag force (F_D) equation $F_D=0.5C_DA_f\rho v_0^2$ where A_f is the presented area of the object, and therefore apply to any fluid including water. However, underwater propagation of fragments may include additional mechanisms such as surface cavitation.

For the present calculations, the largest fragment is assumed to travel the farthest with a shape factor k of 0.25 times the density of steel for a typical casing fragment [2], and a density of 1 g/cc for water or 1.2 kg/m^3 for air as appropriate. Both the fragment shape and Reynolds number (Re) were considered to determine the drag coefficient C_D. With Re above 10^6 and Mach numbers below one, the fragments were subjected to drag in the subsonic turbulent regime. Using a tumbling face-on cube as an approximation of the fragment, a C_D of about one [8] was assumed for the calculations. The range calculated using the Gurney velocity of

730 m/s (Eq. 1) is denoted R_{Gurney}, and the range calculated using the measured fragment velocity of 196 m/s is denoted R. Maximum underwater ranges of 56-71 cm and 39-51 cm were found using the Gurney velocity and the measured velocity respectively. Ranges in air of 200-300 m are shown for comparison. As expected, the hazardous fragment range is very limited underwater.

An alternate method of calculating the hazardous range of an underwater fragment can be found in a Swisdak's report [2]. It was observed from explosion tests involving underwater Mk-82 bombs that no fragments would exit the water if the bomb was located at a scaled depth of more than 1.59 $m/kg^{1/3}$ (4 $ft/lb^{1/3}$). For a 143 g C4 charge this critical depth was found to be 72 cm. This compares favorably to the ranges (particularly R_{Gurney}) calculated in Table 1, indicating that fluid drag provides the main opposing force to fragment propagation underwater.

Further analyses of the fragments revealed a non-Gaussian size distribution, as shown by the histograms in Figure 7, Figure 8, and Figure 9. The distributions show a large population of small fragments, and a smaller population of large fragments. This type of distribution has characteristics of a bi-linear probability trend commonly found in fragmentation processes involving high strain rates such as hyper-velocity impact or explosions.

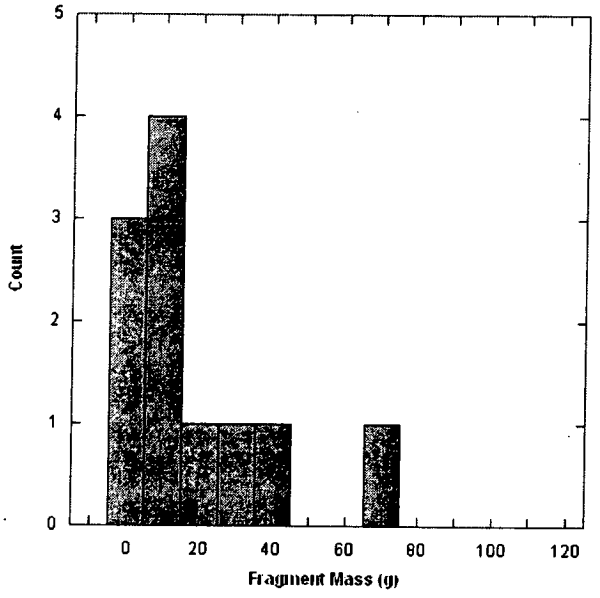

Figure 7. Fragment size distribution for first underwater test.

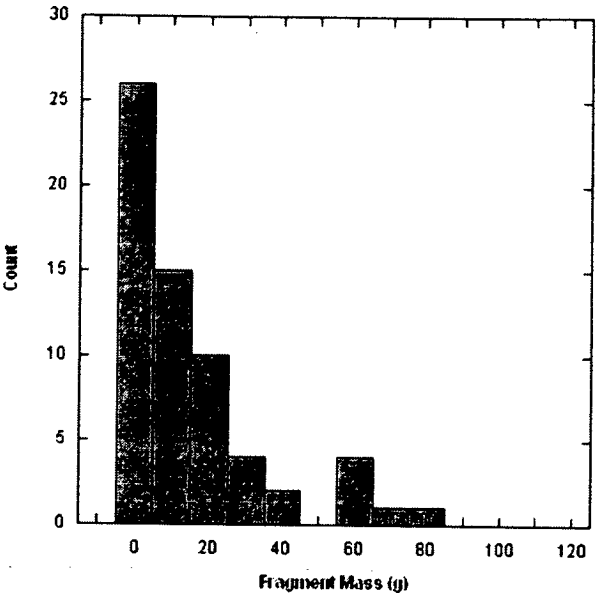

Figure 8. Fragment size distribution for second underwater test.

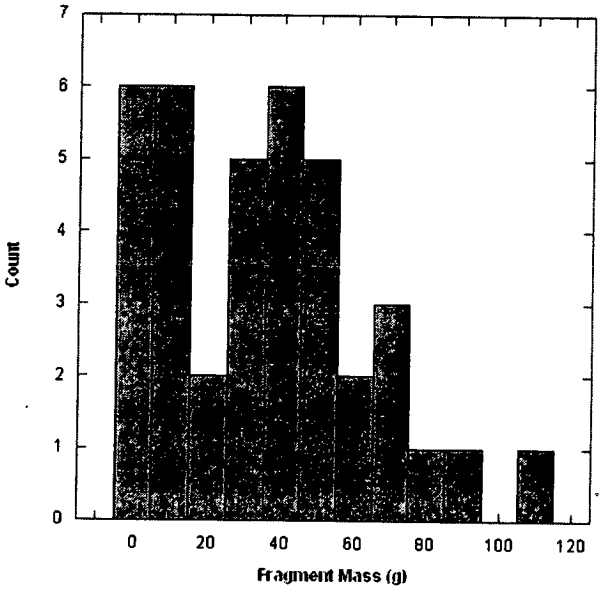

Figure 9. Fragment size distribution for third underwater test.

The probability distribution curves for the fragments are shown in Figure 10, where a point on a curve indicates the percentage of fragments smaller than that size. Tests 1 and 2 show a similar slope in the larger fragment range, while test 3 shows a slope similar to test 4 in air, only shifted to a larger size. These two latter curves also show a knee and change of slope in the middle of the curve indicating features of a bi-linear distribution. A Mott fragmentation distribution is calculated for comparison. The Mott distribution, as revisited by Crull [7], is given by the number of fragments N_f larger than a given fragment mass W_f.

$$N_f = \frac{8W_c e^{-\left[\sqrt{W_f}/M_A\right]}}{M_A^2} \tag{4}$$

where the distribution function M_A is:

$$M_A = Bt_c^{5/6} d_i^{1/3}\left(1+\frac{t_c}{d_i}\right) \tag{5}$$

and W_c is the casing mass, B is the Mott constant, t_c is the casing thickness, and d_i is the inner diameter of the casing. Eqs. 4 and 5 are in units of *ft* and *lb*. The Mott constant could not be found for C4 explosive, and was estimated at 0.8 $lb^{1/2}/ft^{7/6}$ based on similar RDX-based explosives. The Mott distribution curve in Figure 10 is significantly lower than experimental probability curves, and converges towards the experimental curves for larger fragments. This suggests that the experimental results are weighted towards larger fragment sizes. The loss of smaller fragments during the collection process causes them to be under-represented in the distribution curves.

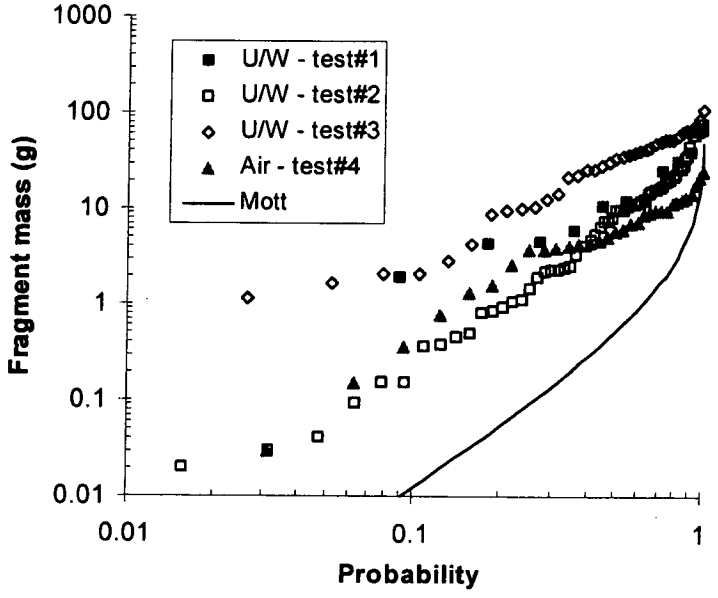

Figure 10. Probability distribution curves for explosion fragments.

Free-field Pressure

The free-field underwater shock pressure was measured for the 2nd and 3rd underwater tests. A typical exponentially decaying curve was observed (Figure 11). Near the tail end of the decay, the pressure is cut off due to the formation of cavitation from rarefaction waves from the surface. The peak pressure agrees very well with the value of 4633 psi obtained from scaling relations for bare charges [5], indicating that the casing had little effect on the peak pressure.

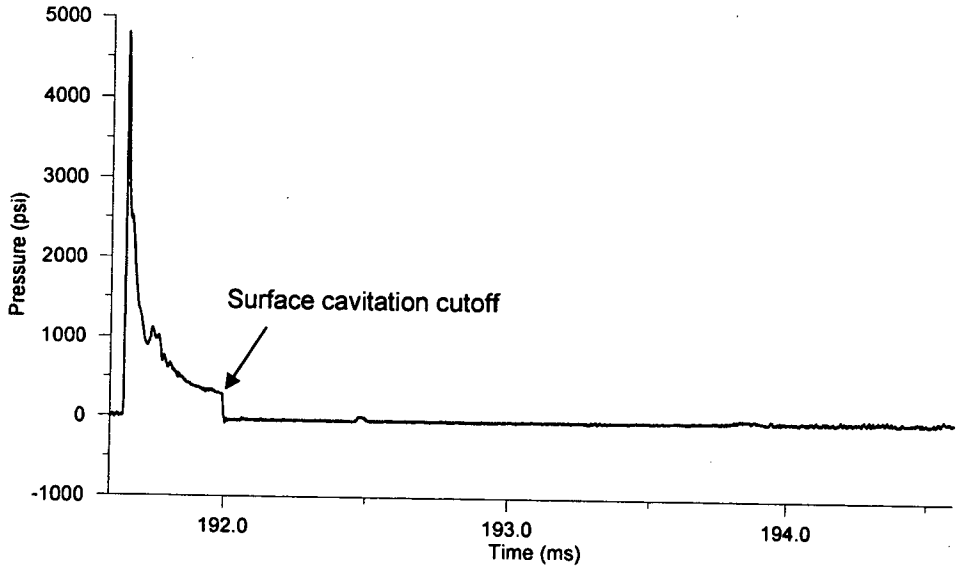

Figure 11. Free-field pressure at a distance of 80 cm from the charge in the 3rd underwater test.

SUMMARY AND CONCLUSIONS

The present investigation of fragmentation properties of underwater charges shows that casing fragments appear to pull ahead of the detonation product bubble early in the explosion process at about 100-200 μs from charge initiation. After rapidly decelerating within a few centimeters, they follow the flow driven by the natural bubble expansion at a relatively low speed of about 200 m/s. At this velocity, larger fragments can still carry enough kinetic energy to cause damage to a target. Underwater drag calculations yield a maximum fragment range of about 70 cm, which agrees well with critical scaled depth calculations. Although the fragment range is limited, the fact that it is dominated by fluid drag suggests that a charge designed to produce abnormally large fragments may have a larger range of damage.

Analyses of the fragment sizes reveals that the largest fragment underwater is 3-4 times larger than the largest fragment for an identical charge detonated in air. The size distributions show features of a typical bi-linear distribution commonly observed for explosively generated fragments, however the loss of small fragments due to the collection method was found to weigh the distributions towards larger sizes.

ACKNOWLEDGEMENTS

The authors gratefully acknowledge early support from the Technical Support Working Group (TSWG), as well as support from field testing (FOS) and explosives handling (ESEG) groups at Suffield.

REFERENCES

[1] Ford, M., and Crull, M., 2000, "Fragment Suppression by Water in Ordnance Disposal Operations", Proc. 29th DDESB Seminar, New Orleans.

[2] Swisdak, MM, Montanaro, PE., 1992, Airblast and fragmentation hazards produced by underwater explosions, Naval Surface Warfare Center, Dahlgren Division, Technical Report NSWCDD/TR-92/196.

[3] Slater, JE, Rude, G., 2004, "Determination of Abovewater Safety Template Distances for Underwater Explosive Ordnance Disposal Activities", To be published as a DRDC report.

[4] Weber, C., 2006, "Maritime Terrorist Threat", New York State Office of Homeland Security. New York, NY.

[5] Paulgaard, G, Slater, JE, and Rude, G., 2004, "Experimental Underwater Explosive Performance of C4", Submitted to be published as a DRDC report.

[6] Dobratz, BM, Crawford PC., 1985, "LLNL Explosives Handbook – Properties of chemical explosives and explosive simulants", United States Department of Energy Facsimile report, UCRL-52997 Change 2, Distribution category UC-45, DE85 015961.

[7] Crull, M. and Opichka, S., 2002, "Hazardous Fragment Distance Calculations for Multiple Rounds", Proc. 30th DDESB Seminar, Atlanta.

[8] Cooper, PW, 1996, Explosives engineering", Wiley-VCH, NY,NY, pp-399-403.